COMPUTERS AND BIOMEDICAL RESEARCH 13, 522–548 (1980)

Determination of Left Ventricular Contours: A Probabilistic Algorithm Derived from Angiographic Images

WILLIAM A. BARRETT, PAUL D. CLAYTON, AND HOMER R. WARNER

Department of Medical Biophysics and Computing, University of Utah, Salt Lake City, Utah 84112

Received March 12, 1980

A probabilistic algorithm for automated left ventricular contour detection is developed which uses information extracted from a variety of angiographic images. These images serve as a training set for the development as well as the evaluation of the algorithm. The algorithm consists of four separate edge detectors combined in a product, each of which is described by a unique probability function derived from the training images. These functions are optimally designed to detect the endocardial border in left ventricular angiograms. A flexible template or model of the left ventricle is constructed from key anatomical features found in the training images and provides global guidance to the edge detection process. The algorithm requires less than 10 sec per contour and a comparison of hand-traced and computed contours shows over 90% of computer-determined coordinates to lie within the interval of reproducibility for manually traced contours.

INTRODUCTION

Left ventricular angiography has gained widespread clinical acceptance in cardiac catheterization centers as an important diagnostic tool in the assessment of heart function in normal and diseased states. The extraction of left ventricular contours from angiographic recordings has greatly facilitated quantitative analysis of cardiac structure and dimensions (*1–5*). If contour data is to be used for studying regional myocardial motion, multiple images throughout the cardiac cycle must be analyzed. As a result, a complete description of ventricular performance involves processing of a vast amount of data. The time and effort required to obtain these data by manual methods has stimulated interest toward the development of partially or totally automated computing techniques for the detection and analysis of left ventricular contours (*6–14*).

Because of the wide variation in ventricular shape, size, and orientation, and because of inconsistencies introduced by intervening structures such as ribs and diaphragms, algorithms which define the contour in one case may prove to be inadequate for another. Thus, left ventricular contour detection remains a difficult problem, requiring excessive manual intervention or processing time. Extraction of outlines in general is easier if one has a priori information derived

0010-4809/80/060522-27$02.00/0
Copyright © 1980 by Academic Press, Inc.
All rights of reproduction in any form reserved.

perhaps from an explicit model of the situation or problem under consideration (*15, 16*). In fact, edge detection schemes which do not incorporate prior information about the type of edge or structure being sought are often unable to distinguish between relevant and irrelevant edges. As a result, when an error has been made, edges which are highly dependent on previously detected edge points tend to propogate that error.

Chien and Fu (*17*) have constructed an algorithm for finding the heart boundary in PA chest radiographs. Prior or global information which incorporates certain assumptions about continuity and curvature of the cardiac structure was used to guide the local detection of boundary points. It was suggested that a general rule for implementing a priori information into the edge detection process might involve flexible template matching or a "rubber mask" technique. That is, certain attributes or features of the structure which remain invariant under rotation, translation, scale change, difference in contrast, or so-called "rubber-sheet distortion" might be used to define a general purpose template which could be adapted and used to guide the edge detection process in the particular image at hand.

The purpose of this paper is to describe a probabilistic algorithm for automated contour detection which uses a priori information extracted from a variety of left ventricular angiographic images. This information consists of video intensity properties and anatomic parameters associated with the manually defined ("true") contour in each of these images. Thus, the images function as a training set for the development as well as the evaluation of the border algorithm.

The Training Images

Ten left ventricular images of varying size, shape, and contrast were selected from an extensive video tape library for inclusion in the training set. Criteria for selection of angiograms included those from which a left ventricular border could be determined by manual methods and the absence of extrasystoles during at least one cardiac cycle. An end-diastolic frame was chosen from each of the ten sequences and a rectangular window surrounding the ventricular silhouette was specified by seven manually entered points (Fig. 1) used to initialize the digitization process (*7, 18–20*). For each of these images the ventricular outline was traced by hand and stored on digital tape with the digitized image and the coordinates of the seven manually entered points. Storage on digital tape assures reproducibility in accessing a particular image in the training set.

Development of the Template and Probabilistic Algorithm

The development of the algorithm is described in three parts:

(1) A flexible piecewise parabolic template which approximates the shape of the left ventricle at end-diastole is derived using a least-squares quadratic fit to given segments of the manually defined contours in each of the training images.

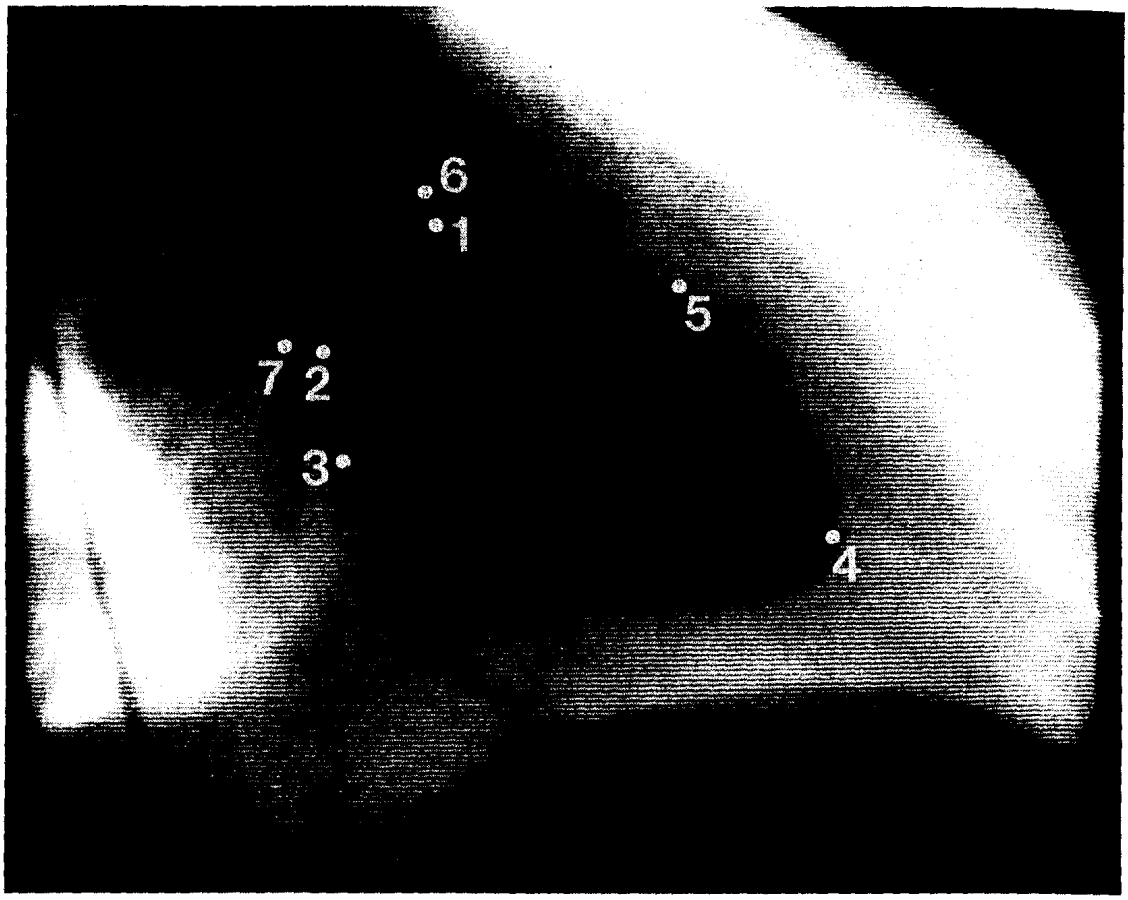

FIG. 1. Video Display of a Left Ventricular Angiogram in the Right Anterior Oblique (RAO) position. Points required to define the digitization matrix are superimposed.

(2) Probability functions are then generated from a quantitative comparison of the template and video data in the images with the location and video information specified by the manually traced contours.

(3) These functions are incorporated into a probability product which allows simultaneous application of several border-defining criteria.

Derivation of the Segmental Parabolic Template

The seven points required to define the digitization matrix are indicated in Fig. 1. Points 1 and 2 are entered at the base of the aortic valve. A 45° line is automatically drawn above the base of the valve and points 6 and 7 are entered where the line and the edges of the aortic silhouette coincide. These points are used as a starting location by the border algorithm. Point 3 is located approximately at the tip of the mitral valve and defines the digitization limits for the left-hand side of the matrix. The lower limit is defined by the apex of the ventricle and is indicated by point 4. The right-hand side of the matrix is determined by the fifth point. The width of the digitization window (specified by points 3 and 5) is actually increased by 20 pixels to allow for the engagement of filters in the border detection algorithm.

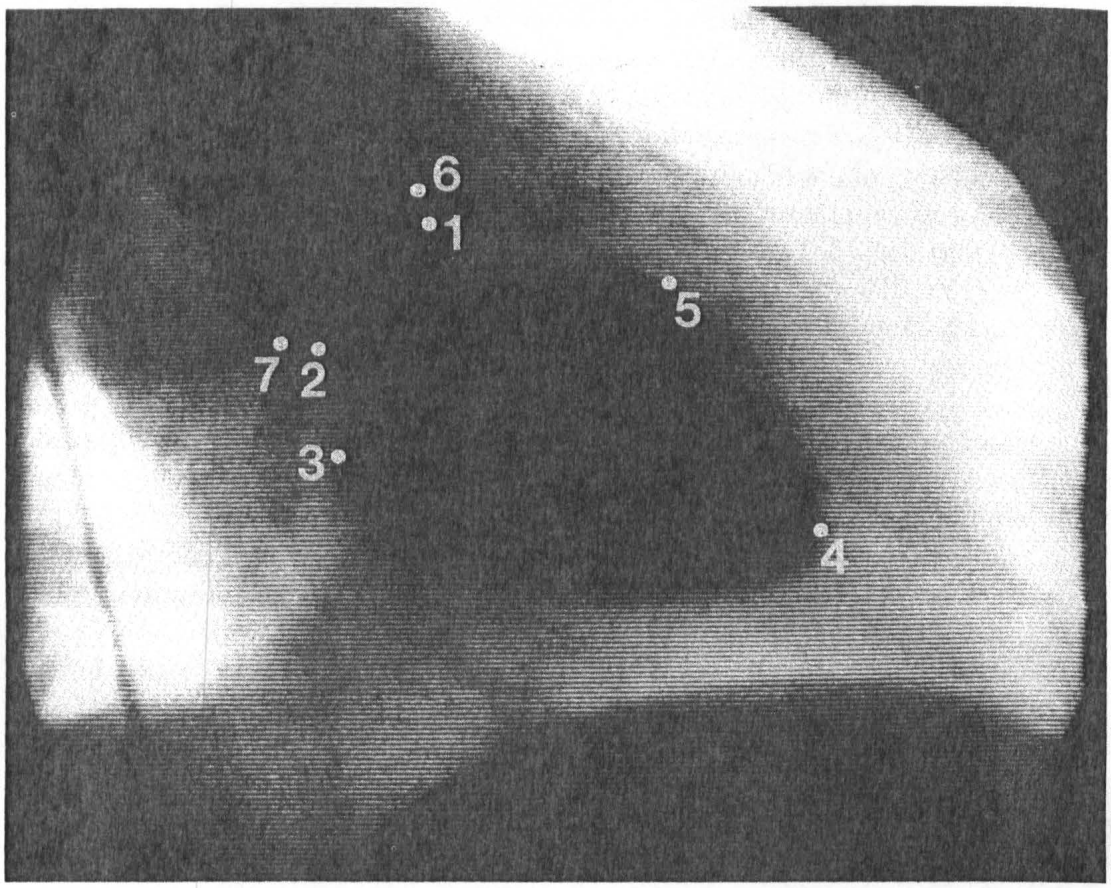

FIG. 1. Video Display of a Left Ventricular Angiogram in the Right Anterior Oblique (RAO) position. Points required to define the digitization matrix are superimposed.

(2) Probability functions are then generated from a quantitative comparison of the template and video data in the images with the location and video information specified by the manually traced contours.

(3) These functions are incorporated into a probability product which allows simultaneous application of several border-defining criteria.

Derivation of the Segmental Parabolic Template

The seven points required to define the digitization matrix are indicated in Fig. 1. Points 1 and 2 are entered at the base of the aortic valve. A 45° line is automatically drawn above the base of the valve and points 6 and 7 are entered where the line and the edges of the aortic silhouette coincide. These points are used as a starting location by the border algorithm. Point 3 is located approximately at the tip of the mitral valve and defines the digitization limits for the left-hand side of the matrix. The lower limit is defined by the apex of the ventricle and is indicated by point 4. The right-hand side of the matrix is determined by the fifth point. The width of the digitization window (specified by points 3 and 5) is actually increased by 20 pixels to allow for the engagement of filters in the border detection algorithm.

Since points 1 through 7 must be entered manually, it is convenient to use them to construct a template or model for approximating the shape of the left ventricle. We begin by connecting (linear interpolation) these points (point 5 in Fig. 1 is not used) with five straight lines. To clarify this procedure, the piecewise linear approximation is shown superimposed on a ventricular outline without the image in Fig. 2a. Since the windowed portion of the angiogram was digitized at a 45° angle (*7*), the corresponding contour appears tilted. A curvilinear model is constructed by using the orthogonal distance between the linear approximation and the actual border as the basis for a parabolic rather than a linear interpolation across each of the segments (labeled L1, L2, L3 and R1, R2; L = left, R = right). This is illustrated in Fig. 2b where the lower third segment, L3, of the left-hand side (inferior wall) has been isolated. Calculation of the orthogonal distance, T, is accomplished by defining a new coordinate system (x', y') with respect to the linear approximation and the origin, 0, of that segment. The xy-axis has been rotated through an angle θ with the origin, 0,

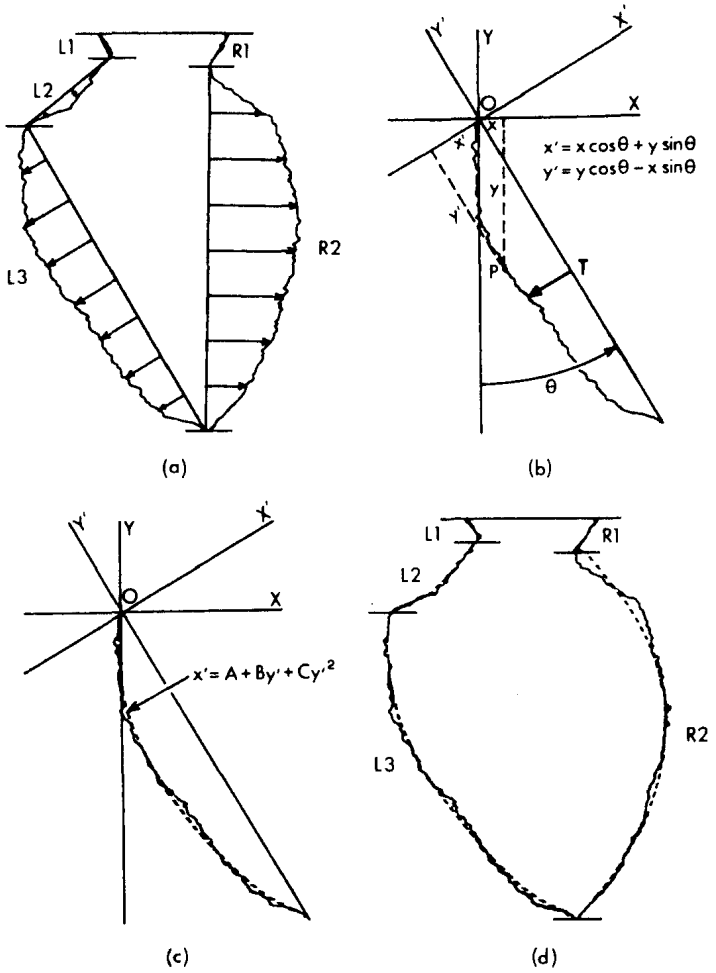

FIG. 2. (a) Hand-traced border with segmental linear approximation superimposed. (b) Rotated coordinate system for calculation of orthogonal distances between hand-traced border and linear approximation. (c) Least-squares parabolic fit to segment L3. (d) Segmental least-squares parabolic approximation to ventricular outline.

remaining fixed. A point P, on the contour with original coordinates (x, y) is now defined by the new coordinates (x', y'), where the orthogonal distance, T, is simply x' (Fig. 2b). By calculating orthogonal distances, an array of $x'y'$-coordinates representing that segment of the contour is constructed and the method of least-squares is used to fit a parabola to the values in the array (Fig. 2c). A parabola is fitted to each of the five segments in this way, resulting in a segmental parabolic approximation to the entire ventricular outline (Fig. 2d). This approximation is refined by a smoothing operation which provides continuity at the juncture of the parabolas. In order to arrive at a uniform coordinate system for describing the piecewise parabolic outline, each of the individually generated $x'y'$ systems are transformed back to the original xy-coordinate system, resulting in a complete quadratic equation of the form

$$Ax^2 \pm Bxy + Cy^2 \pm Dx + Ey = 0 \qquad [1]$$

for each of the five segments. The sign, where $\pm$ is indicated, is dependent upon rotation of the axis (linear approximation, Fig. 2a) through either a positive or negative angle.

Figures 2d and 3a indicate that hand-traced end-diastolic contours can be well-approximated by five connected parabolas. However, for a newly encountered left ventriculogram a hand-traced border is not available. Assuming that the 10 contours derived from the training set are representative, they can serve as a basis for an "average" segmental parabolic approximation, which can then be applied to a new image. An "average" parabolic approximation is obtained by combining data extracted from all 10 training contours. For each segment the orthogonal distance between the linear approximation and the hand-traced border is calculated and stored in an array. Calculation of these distances for each of the training contours produces 10 arrays for each segment. Since the contours and their respective segments differ noticeably in absolute size from one to another (Fig. 3), arrays corresponding to a given segment are normalized to a fixed length. The average of all 10 values at each position in the array is computed to form an averaged array. This procedure is followed for each segment, producing five averaged arrays. The method of least-squares is again used to fit a parabola to each of the averaged arrays. The coefficients of the quadratic equation describing the averaged segmental parabola in Eq. [2] define a general segmental parabolic approximation which can be applied to that particular segment in any of the original 10 contours, or more importantly, in a newly encountered left ventriculogram:

$$\bar{X} = \bar{A} + \bar{B}y' + \bar{C}y'^2. \qquad [2]$$

The general parabolic approximation or template of the ventricle consists of five averaged parabolas and can be compactly described by 15 coefficients. The general template is not as optimally suited to each of the training contours as those derived separately (Fig. 3a), but does provide a reasonable approximation to those contours (Fig. 3b).

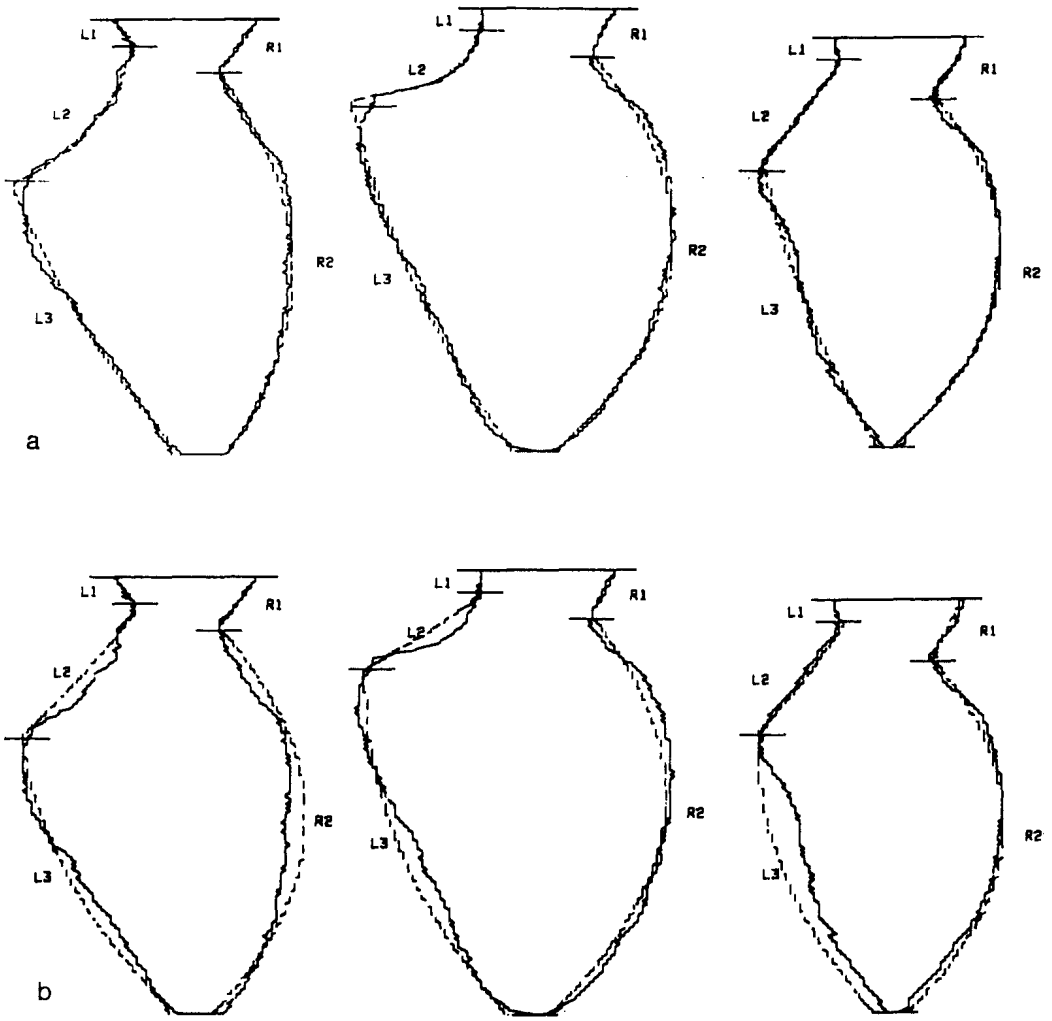

FIG. 3. (a) Least-squares parabolic approximation (dashed line) to training contours 1, 4, and 5. (b) General parabolic approximation (dashed line) to training contours 1, 4, and 5.

The Probabilistic Parabolic Template

The template can also be used to define a probable search interval for the ventricular border. Figure 4a shows the general parabolic fit to the contour described in Fig. 2. The differences (not orthogonal) between the two borders are calculated by subtracting the parabolic border coordinates from the hand-traced border points on each line. A histogram of the differences is generated for each of the five segments and shown for segment L3 in Fig. 4b. The histogram describes the relative frequency as well as the magnitude and direction by which the manually traced border differs from the parabolic approximation. A deviation of zero and the range of the histogram are indicated along the horizontal axis.

Segmental histograms are generated in the same way for all 10 training contours, producing a total of 50 histograms. Histograms corresponding to

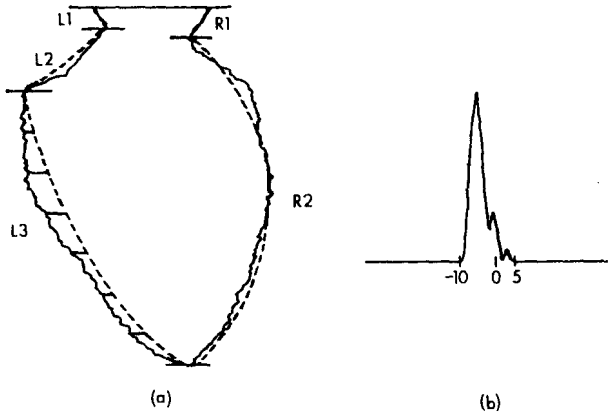

FIG. 4. (a) Hand-traced border with general parabolic template (dashed-line) superimposed. (b) Histogram generated by subtracting parabolic coordinates from corresponding hand-traced values in segment L3.

each segment are normalized and summed to form five "pooled" distributions (Fig. 5). The pooled distributions describe the relative frequency of the contour location with respect to the general parabolic template in a given segment of the training images and can be considered probability density functions when the number of observations is made large. For this reason the number of contours in the training set will be increased. When the probability distributions in Fig. 5 are aligned with respect to their "zero deviation marks" on their corresponding segmental parabolic approximations, they describe the probability that the true border lies at each point with respect to that particular parabolic template.

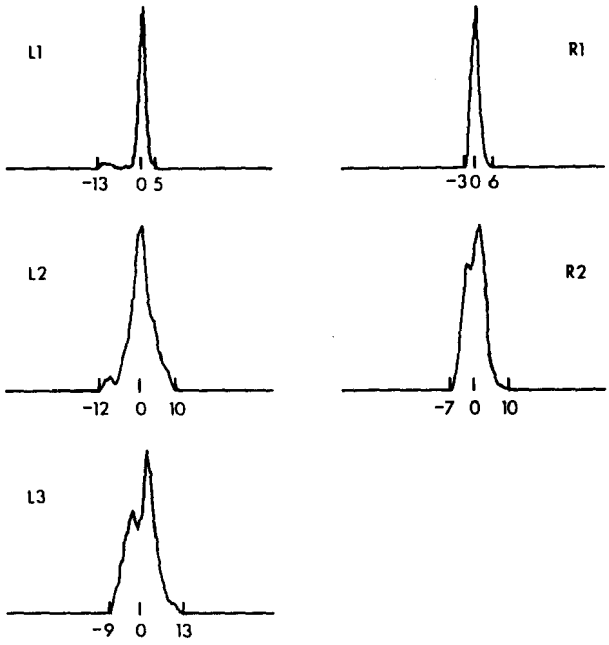

FIG. 5. Pooled segmental histograms generated from training contours 1–10. Distributions L1, L2, L3, and R1, R2 are the probability functions for the general parabolic template. x-Axis = pixel units, y-axis = probability.

Clearly the probabilistic parabolic template would not be sufficient in itself to identify the location of the ventricular contour, since the most probable location would always be the maximum value of the distribution. This would simply locate the border a fixed distance from the template. However, when used in conjunction with other probabilistic terms it serves three purposes:

(1) The width of the distribution in a given segment limits the search interval and constrains the border to lie within those limits. The probability of finding the border outside of this range is zero since no border points were ever encountered that far away in the training set. This automatically eliminates time and effort associated with unproductive searching outside of the prescribed interval. The need then, for an exhaustive training set, (more than 10), becomes obvious.

(2) It not only constrains the border to lie within the interval but also gives the most probable location within that interval.

(3) It contains information based on global characteristics which allows for intelligent border prediction to continue when the ventricular outline becomes indistinguishable over small segments or when other border-defining criteria become insensitive to existing video information (i.e., when the ventricular outline is obscured by a rib or diaphragm).

The extent to which a single parabola can adequately characterize a given segment in any of the 10 contours can be determined by examining the amount of dispersion in the distributions shown in Fig. 5. The data in Table I indicate, for each segment, the percentage of points from the general parabolic template which coincided with border coordinates from the hand-traced contours, as well as the percentage which differed from the hand-traced contours within a range of ±4 points. The data show that while there was coincidence between the

TABLE I

COMPARISON OF GENERAL PARABOLIC APPROXIMATION WITH HAND-TRACED BORDERS FOR CONTOURS 1–10

	Interval around hand-traced contour[a]					
Segment	0	±1	±2	±3	±4	>±4
L1	58.0	88.9	91.6	91.9	93.2	6.8
L2	19.0	48.7	67.1	80.6	89.1	10.9
L3	10.3	35.7	60.5	77.2	88.7	11.3
Left side	14.5	40.7	62.7	77.5	88.8	11.2
R1	47.9	95.2	99.6	100.0		0.0
R2	17.4	50.7	80.4	93.1	98.0	2.0
Right side	20.0	55.0	82.1	93.7	98.1	1.9
Total	17.3	47.8	72.4	85.6	93.4	6.6

[a] 1 pixel ≅0.5 mm

Note. The table shows the percentage of parabolic points within given intervals.

hand-traced border and the parabolic approximation only 17.3% of the time, the parabolic template was within ±4 points of the hand-traced contour 93.4% of the time. Even with the inclusion of an additional 10 contours, over 90% of the parabolic coordinates were within ±4 points, or approximately 2 mm, of the hand-traced contours.

The suitability of a single parabola, as opposed to some other polynomial, for characterizing these segments can be determined by examining the coefficients (Fig. 2c), of the parabolas which were generated individually (Figs. 2d and 3a).

Of primary concern is coefficient C, which describes the direction and amount of concavity in the parabola. Values of C for segments L3 and R2 were consistent in sign and magnitude throughout the 10 training contours. This is significant since segments L3 and R2 identify respectively the inferior and anterior free wall, or the contracting portion of the ventricle.

Parabolas for segments L1 and R1 exhibited curvature to both sides of the vertical axis, although the corresponding distributions in Fig. 5 are quite narrow. This indicates that these segments could probably be well approximated by a straight line. Segment L2 is similar to L1 and R1 in that concavity to either side of the axis was observed. This resulted in a parabola corresponding roughly to a straight line. Approximation of the mitral valve segment with a straight line is a technique often used in the manual outlining of contours, since the shape of the mitral valve does not contribute significantly to the analysis of ventricular wall motion.

These data, and those displayed in Table I indicate the general parabolic template to be suitable for approximating the shape of the left ventricular outline in end-diastolic frames.

The Probability Product Approach to Border Recognition

A detailed description of the algorithm which uses a probability product approach is given by Clayton *et al.* (*7*). The algorithm consists of four border-defining terms which are combined in a product to represent the likelihood that a particular point along a given line of the digitized matrix should be designated as the border point. Equation [3] gives the likelihood that the ith point along a given line is the right-hand border for that particular line:

$$\begin{matrix}\text{Product}\\ \text{Right}(i)\end{matrix} = \begin{matrix}\text{Matched}\\ \text{Gradient}\\ \text{Filter}(i)\end{matrix} * \begin{matrix}\text{Video}\\ \text{Level}\\ \text{Predictor}(i)\end{matrix} \quad \begin{matrix}\text{Location}\\ \text{Predictor}(i)\end{matrix} * \begin{matrix}\text{Sequence}\\ \text{Predictor}(i)\end{matrix}, \qquad [3]$$

The predicted right-hand border coordinate for this line is that value for which Product Right(i) is a maximum. The border for the left side of the ventricle is found in a similar manner.

The first term in the product, the "Matched Gradient Filter," employs the concept of spatial differentiation, where the border is assumed to lie in regions

of rapidly changing intensity. In order to achieve more sensitivity at low light intensities which are encountered at the ventricular border a logarithmic transformation is performed before differentiation (*19*). The derivative of the densities is computed across an entire line and then convolved with a 12-point Gaussian curve which is assumed to match the derivative of the density gradient at the border. This is done for each point on the line and the maximum value for this term occurs where the line derivative most closely matches the Gaussian curve.

The second term, the Video Level Predictor, uses the video level of the border point on the preceding line to predict the video level at the border point on the present line. The video level most closely approaching this predicted value has the highest likelihood of being on the ventricular border according to this term.

The location term predicts the border on the present line to be the same position as it was on the preceding line. This is based on the assumption that marked discontinuities in the border between successive lines do not exist.

The sequence predictor extracts information from the temporal movement of the ventricular border. For a given line, the absolute difference in the border coordinates in the previous two video fields is used to predict the location of the border in the current video field by extrapolation.

The parabolic template with its associated probability functions is now included in the product

$$\begin{matrix}\text{Product} \\ \text{Right}(i)\end{matrix} = \begin{matrix}\text{Matched} \\ \text{Gradient} \\ \text{Filter}(i)\end{matrix} * \begin{matrix}\text{Video} \\ \text{Level} \\ \text{Predictor}(i)\end{matrix} * \begin{matrix}\text{Location} \\ \text{Predictor}(i)\end{matrix} * \begin{matrix}\text{Quadratic} \\ \text{Predictor}(i)\end{matrix}, \quad [4]$$

where it is referred to as the Quadratic Predictor, due to the quadratic nature of the parabolic template. In practice the Sequence Predictor in Eq. [3] cannot be used until at least the end-diastolic contour has been determined.

Rather than empirically weighting the effect of the other terms in the algorithm, as has been done previously, it is desirable to generate for each of them probability functions based on the contour and video information in the training set, as was done for the Quadratic Predictor.

Generation of Probability Functions for Algorithmic Terms

The Matched Filter Probability Functions

Probability functions for this term are generated in such a way that the Matched Filter will not only maximize a gradient, but particularly the gradient found at the hand-traced border in the training images. This is accomplished by normalizing the Matched Filter Output (convolution of the Gaussian curve and line derivative) at the border to a percentage of the sum of the Matched Filter Outputs six points to either side of the manually defined border on the

preceding line

$$\begin{matrix}\text{Normalized} \\ \text{Matched Filter} \\ \text{Output}(B)_L \\ (\%)\end{matrix} = \left[\frac{\text{M.F. Output } (B)_L}{\sum_{i=-6}^{+6} \text{M.F. Output } (B + i)_{L-1}}\right] * 100, \qquad [5]$$

where $B = x$ value of manually entered border coordinate and L = line number.

Normalization of the Matched Filter Output by this area under the curve produces consistent values in spite of the varying intensity gradients found in different images. The Matched Filter Output curve from the preceding line is used for normalization, since, due to the nature of the 12-point convolution, the sum of the outputs is not yet available at the time the border point is reached on the present line. Since the gradient does not differ significantly from line to line, the output curve on the preceding line is assumed to provide a suitable approximation for that found on the present line.

Histograms of the Normalized Matched Filter Output are generated for each segment in each of the ten training images, and scaled to 1000 in each case. Then, as with the Quadratic Predictor, histograms corresponding to given segments are summed to produce five pooled distributions, indicated by the cross-hatched areas in Fig. 6. The pooled distributions are the probability

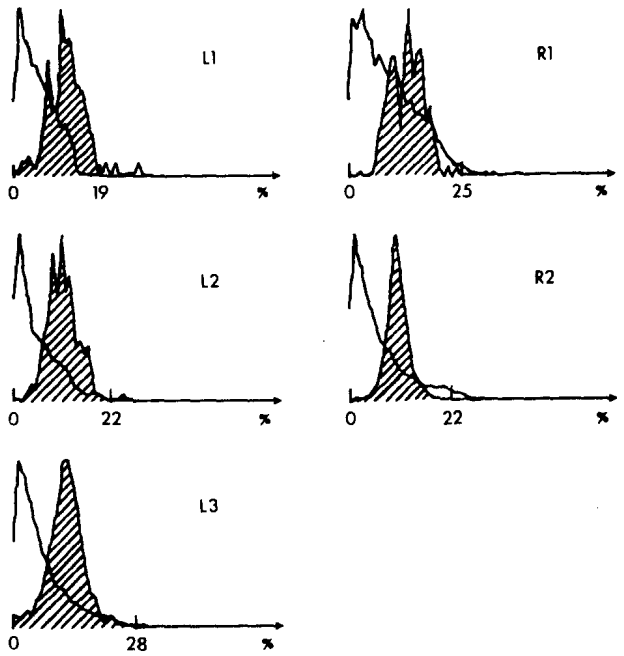

FIG. 6. Pooled probability distributions for the Matched Filter Predictor (indicated by cross-hatched areas). Superimposed are pooled distributions of the Matched Filter Output for every point on the line as a percent of the sum of the Matched Filter Outputs six points to either side of the border. x-Axis = percentage, y-axis = probability.

functions for the Matched Gradient Filter in Eq. [4]. Superimposed on these functions for illustrative purposes are the Normalized Matched Filter Outputs pooled from every point on the line, rather than only at the border. The noticeable separation between the two distributions shows that Matched Filter Outputs at the border can be discriminated from lower, and more importantly, from misleading high outputs which occur elsewhere in the image.

For a newly encountered ventriculogram, the probability functions in Fig. 6 are used in the following way. The Matched Filter Output is calculated for each point on line L and normalized using Eq. [5] to a percentage of the 12-point interval defined by the computer-determined border in the preceding line. The computer-determined border must be used since a manually entered border coordinate, B, is not available. The probability for the normalized value is obtained from the probability function associated with the segment in which line L is located. For example, the probability for a Normalized Matched Filter Output of 10% is that value on the cross-hatched curve (Fig. 6) corresponding to that percentage. This probability is the value to be used for the Matched Gradient Filter term in Eq. [4]. If a line in segment R2 were being processed, the probability would be greatest at approximately 9–10%.

The Video Level Probability Functions

The probability functions for the Video Level Predictor are similar to those created for the Matched Filter Predictor. Histograms are generated by subtracting the predicted video level, specified by the computer-determined border, C, in line L-1, from the video level at the manually entered border on line L (Eq. [6]). The difference is then normalized to a percentage of the contrast or total range of video levels on that line, such that

$$\begin{matrix}\text{Normalized} \\ \text{Video Level} \\ \text{Predictor}(B)_L \\ (\%)\end{matrix} = \left\{ \frac{\text{Video Level}(B)_L - \text{Predicted Video Level}(C)_{L-1}}{\text{Video Level}(\max)_L - \text{Video Level}(\min)_L} \right\} * 100, \qquad [6]$$

where $C = x$ value of computer-determined border coordinate, $B = x$ value of manually entered border coordinate, and L = line number.

Normalization of the difference by contrast eliminates variation in the histogram which would otherwise be introduced by the wide variation in contrast within an image as well as between images in the training set. As before, histograms are derived segmentally and those corresponding to given segments are pooled into five distributions which define the probability functions for the Video Level Predictor. When a new ventriculogram is encountered, the Video Level probability functions are used in the following way. The predicted video level at point C on line L-1 is subtracted from the video level at point i on line L. This difference is normalized to a percentage of the total contrast on line L using Eq. [6]. The probability for that normalized value is found from the function associated with the segment in which line L is

FIG. 7. (a) Original digitized image. (b) Two-dimensional intensity-modulated display of Video Level probability functions corresponding to segments L1, L2, and L3, displayed for each pixel in the matrix. (c) Intensity display of right-hand probabilities (R1, R2). Hand-traced border is superimposed in black.

located, as with the Matched Filter probability functions. This probability is the value to be used for the Video Level Predictor in Eq. [4].

The effect of the Video Level probability functions can be better visualized in the context of a particular left ventricular angiogram (training image 10), which was digitized and displayed using a RAMTEK GX-100 (Fig. 7a). Two-dimensional intensity-modulated displays of probability values associated with

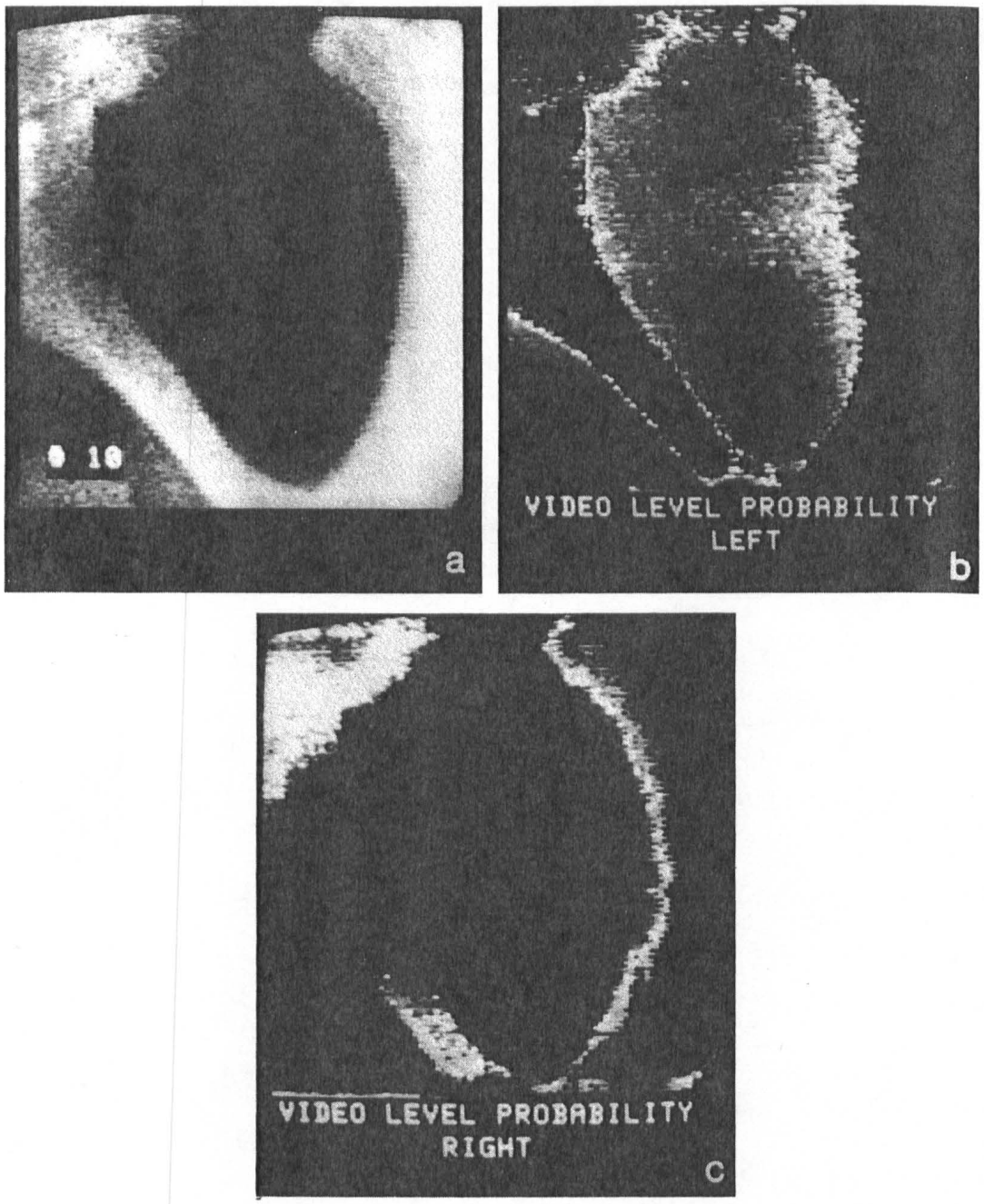

FIG. 7. (a) Original digitized image. (b) Two-dimensional intensity-modulated display of Video Level probability functions corresponding to segments L1, L2, and L3, displayed for each pixel in the matrix. (c) Intensity display of right-hand probabilities (R1, R2). Hand-traced border is superimposed in black.

located, as with the Matched Filter probability functions. This probability is the value to be used for the Video Level Predictor in Eq. [4].

The effect of the Video Level probability functions can be better visualized in the context of a particular left ventricular angiogram (training image 10), which was digitized and displayed using a RAMTEK GX-100 (Fig. 7a). Two-dimensional intensity-modulated displays of probability values associated with

the Normalized Video Level Predictor are created for each point in the digitized matrix (Figs. 7b–c). Figure 7b represents the "left-hand" probabilities defined by functions corresponding to segments L1, L2, and L3 of the inferior wall. Figure 7c is a similar display of the "right-hand" probabilities. High intensities correspond to high probabilities, while the converse is true of low intensities.

The intensity displays provide a means for global assessment of the Video Level Probability functions in a given image, and for comparison of highlighted pixels in regions near the actual border with those found in other areas of the picture. For example, pixels illuminated by left-hand probabilities have almost vanished in Fig. 7c, emphasizing the distinctive characteristics of each set of functions. Two-dimensional displays of probability functions corresponding to other algorithmic terms are generated in the same way.

The Location Probability Functions

The Location Predictor is different from the other terms in the algorithm in that it predicts the border based upon its combined effect with the other terms. As a result, its corresponding probability functions reflect the performance of, and act as a self-correcting feature for the entire algorithm. The probability functions for the Location Predictor are generated in the same way as those for the Quadratic Predictor. Histograms of the differences between hand-traced and computer-determined borders are calculated for each image, normalized,

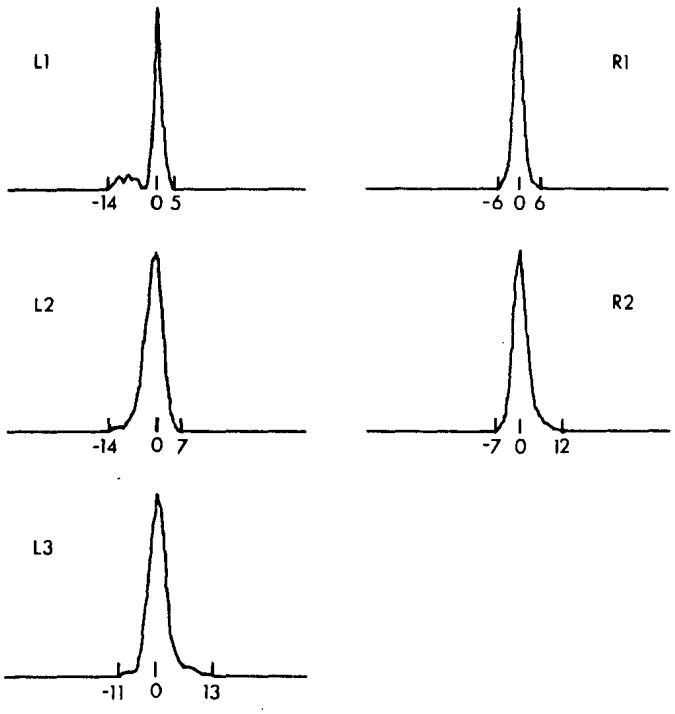

FIG. 8. Pooled segmental histograms generated from training contours 1–10. Distributions L1, L2, L3, and R1, R2 are the probability functions for the Location Predictor. x-Axis = pixel units, y-axis = probability.

and summed into pooled distributions corresponding to each segment. The pooled distributions in Fig. 8 are the probability functions for the Location Predictor.

The probability functions which have been generated for each of the terms in Eq. [4] can now be incorporated in the algorithm. Functions for the Quadratic Predictor (Fig. 5) and the Location Predictor (Fig. 8) are applied directly, by aligning the zero mark on the predicted border point. For the Location Predictor, the predicted border point is the position specified by the computer-determined border in the preceding line. For the Quadratic Predictor the position of the predicted border is defined by the segmental parabolic approximation. Probabilities for the Matched Gradient Filter and the Video Level Predictor are accessed indirectly using normalized values which are computed at each point on the line, as described previously.

The algorithm described by Eq. [4] is illustrated for a given line in Fig. 9a, where probabilities corresponding to each of the four terms have been displayed within the range defined by the Quadratic Predictor. The product of the probabilities at each point is shown in Fig. 9b. The maximum value of the probability product, indicated by line element i, identifies the computer-

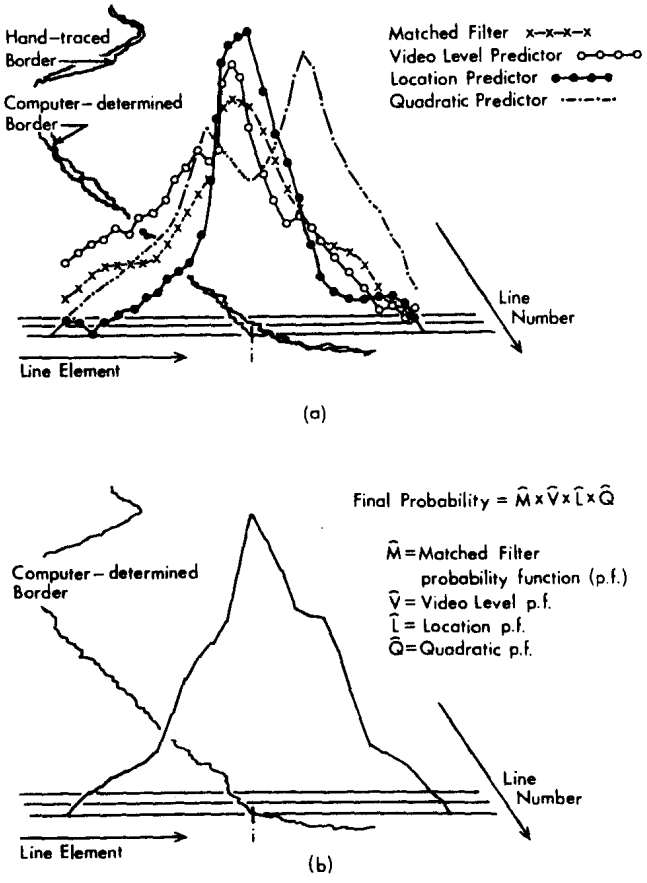

FIG. 9. (a) Probability functions corresponding to algorithmic terms applied to a given line. (b) Product of the functions in (a). Maximum value indicates computer-determined border point for that line.

determined border point for that line. To facilitate reference to the terms with their associated probability functions, the symbolic representations $\hat{M}$, $\hat{V}$, $\hat{L}$, and $\hat{Q}$ are also defined.

The use of a probability product requires that the terms $\hat{M}$, $\hat{V}$, $\hat{L}$, and $\hat{Q}$ be independent (*21*). The question of independence was investigated by performing linear correlations between each pairwise combination of terms ($\hat{M}$–$\hat{V}$, $\hat{M}$–$\hat{L}$, $\hat{M}$–$\hat{Q}$, $\hat{V}$–$\hat{L}$, $\hat{V}$–$\hat{Q}$, and $\hat{Q}$–$\hat{L}$). The coefficient of correlation, r, between the probabilities in each combination was computed for each segment throughout the 10 training images. Mean correlation coefficients, $\bar{r}$, were then generated for each segment in each of the six pairs. Values for $\bar{r}$ ranged from 0.12 to 0.38 with the exception of segments L1, L2, and R1 in the $\hat{Q}$–$\hat{L}$ pair, where values from 0.55 to 0.67 were observed. High correlations between $\hat{Q}$ and $\hat{L}$ might be expected since both terms contain information predicting the curvature of the ventricle, that for $\hat{Q}$ being global, and that for $\hat{L}$, local. However, the much lower values of 0.26 and 0.15 in segments L3 and R2, which define a major portion of the ventricle, emphasize the distinctive features of both terms. The low correlation coefficients found in these and all other pairwise combinations indicate that independence of terms is not an unreasonable assumption.

Refinement of the algorithm described in Fig. 9b is accomplished by optimizing the probability functions derived for $\hat{V}$ and $\hat{L}$. Generation of functions for these two terms requires information about computer-determined contours. As a result, a change in computed contours will produce a different set of functions. For example, the algorithm $\hat{M}*V*L*\hat{Q}$ produced the contours which were used to create $\hat{V}$ and the resulting algorithm $\hat{M}*\hat{V}*L*\hat{Q}$. Similarly, $\hat{M}*\hat{V}*L*\hat{Q}$ was used to obtain $\hat{L}$ and $\hat{M}*\hat{V}*\hat{L}*\hat{Q}$ (Fig. 9b). Refinement of the algorithm continues by using $\hat{M}*\hat{V}*\hat{L}*\hat{Q}$ to create a different and more optimal set of functions, $\hat{V}_2$, for the Video Level Predictor. $\hat{M}*\hat{V}_2*\hat{L}*\hat{Q}$ is then used to create $\hat{L}_2$, and so on.

Iterative processes are not used for $\hat{M}$ and $\hat{Q}$, since the information from which they are derived (hand-traced borders and parabolic templates) is fixed, whereas $\hat{V}_2$ and $\hat{L}_2$ reflect predicted border points in the current stage of algorithm development. Iteration is continued until contours in the training set reach some observable limit where they cease to converge on the hand-traced borders. This occured after the fourth iteration, resulting in the present algorithm, $\hat{M}*\hat{V}_4*\hat{L}_4*\hat{Q}$. Development of the algorithm in this way results in convergence of computer-determined border points to the hand-traced values. The functions which have now been associated with algorithmic terms define actual probabilities which have been derived from the contour and video data in the training set, rather than probabilistic assumptions based on the empirical weighting of constants.

Sequential Border Detection

The algorithm to this point has been applied to contour detection in end-

diastolic images. Extension of the algorithm to contour detection throughout the contractile sequence is also desirable. The Sequence term in Eq. [3] predicts the location of the contour based on assumptions related to the temporal movement of the ventricle, and cannot be applied until the end-diastolic contour has been determined.

Probability functions for the Sequence Predictor are generated using methods similar to those developed for the Quadratic and Location Predictors. Contours which were previously traced by hand (from end-diastole to end-systole, Fig. 10a), yielding approximately 20 contours per angiogram, are used for this purpose. Histograms of the difference between border points on adjacent contours are calculated for each segment and those corresponding to a given segment (L3, for example), are combined to form a single distribution (Fig. 10b). Segmental distributions derived from the 10 hand-traced contour sequences are combined to form pooled distributions (Fig. 10c). The pooled distributions are the probability functions for the Sequence Predictor (Fig. 10d). The probability functions for the Sequence Predictor indicate the movement of the ventricular wall between adjacent contours over all 10 studies. Since very little movement takes place in the 1/60-sec interval between adjacent contours, the resulting functions are quite narrow. This is to be expected for segments L1, R1, and L2, which represent the noncontracting portion of the ventricle. Distributions L1, L2, and L3 are consistently skewed to the right, with the maximum value occuring at 0 for L1 and at +1 for L2 and L3. This illustrates the general inward motion of the inferior wall. Distribution R2 is skewed slightly to the left (by area), although both R1 and R2 have maximum values occuring at 0. Here the effect of the inward motion of the anterior wall appears to be somewhat negated by the rotation of the ventricle. Therefore, cross-hatched areas do not represent purely paradoxical motion but rather, are due primarily to ventricular rotation, and, to a lesser degree, artifact introduced from the manuals tracing of contours.

The Sequence Predictor, S, with its associated probability functions can now be implemented into the algorithm by aligning the functions on the most recent computer-determined border in the sequence after the initial end-diastolic contour has been determined. In other words, the General Parabolic Template is used as an approximation to the first (end-diastolic) frame in the sequence and the most recent computer-determined border is used as an approximation to the contour in succeeding frames. Thus, once the end-diastolic contour has been determined, the algorithm assumes the form described by Eq. [3]. The nature of the sequence functions prevent the contour from diverging and give emphasis to the inward motion of the ventricular wall. Using this algorithm, successive frames recorded on the video disc are advanced and digitized under computer control until the entire contractile sequence has been processed.

Results and Discussion

Using the algorithm, $\hat{M}*\hat{V}_4*\hat{L}_4*\hat{Q}$, contours were computed for each of the 10 training images. Visual results are shown for images 1 and 5 in Figs. 11 a–d,

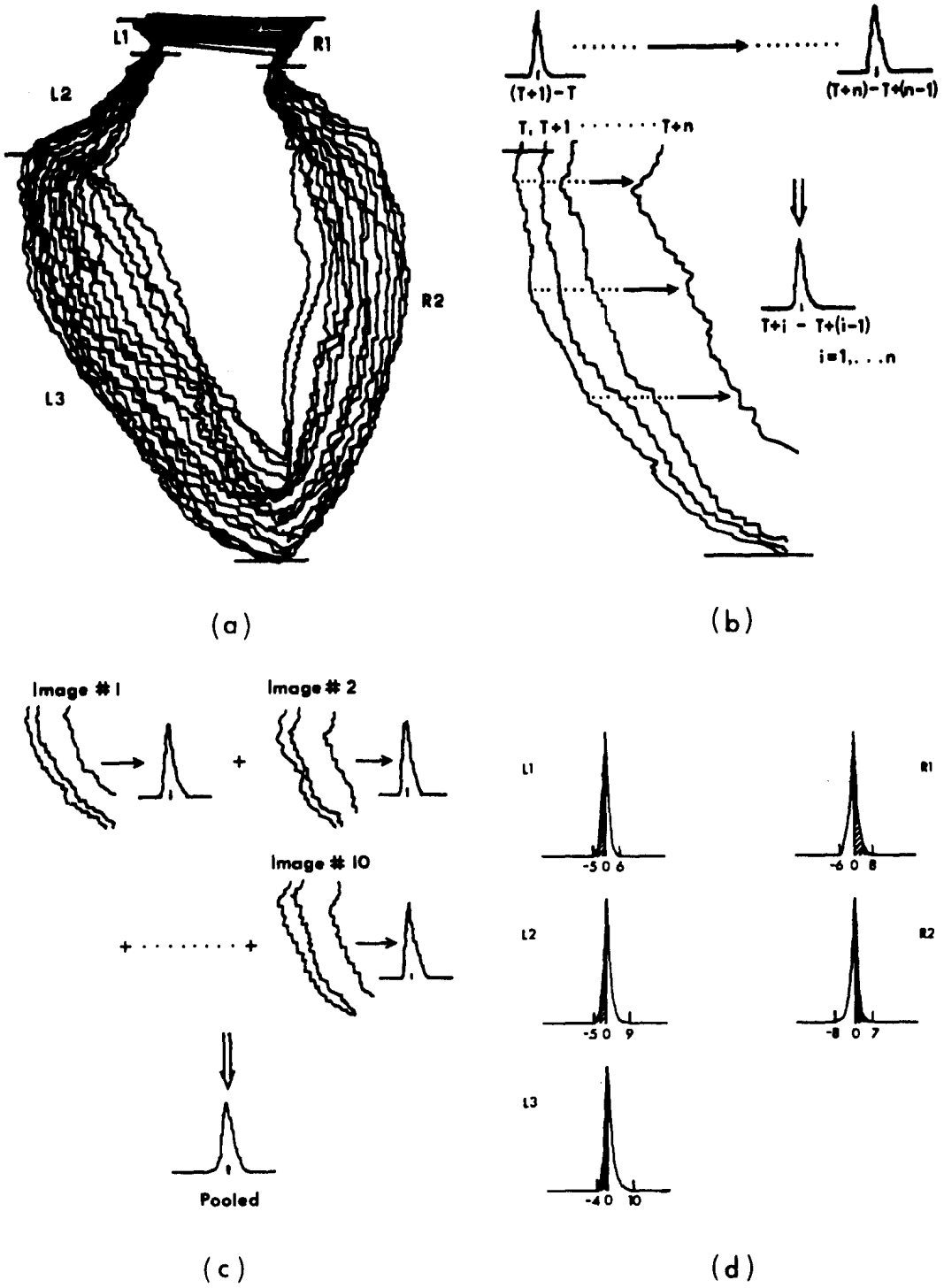

FIG. 10. (a) Hand-traced systolic contours. (b) Segmental histograms generated from subtraction of border coordinates in adjacent contours. (c) Pooled segmental histograms generated from ten different contour sequences. (d) Pooled histograms define the probability functions for the Sequence Predictor.

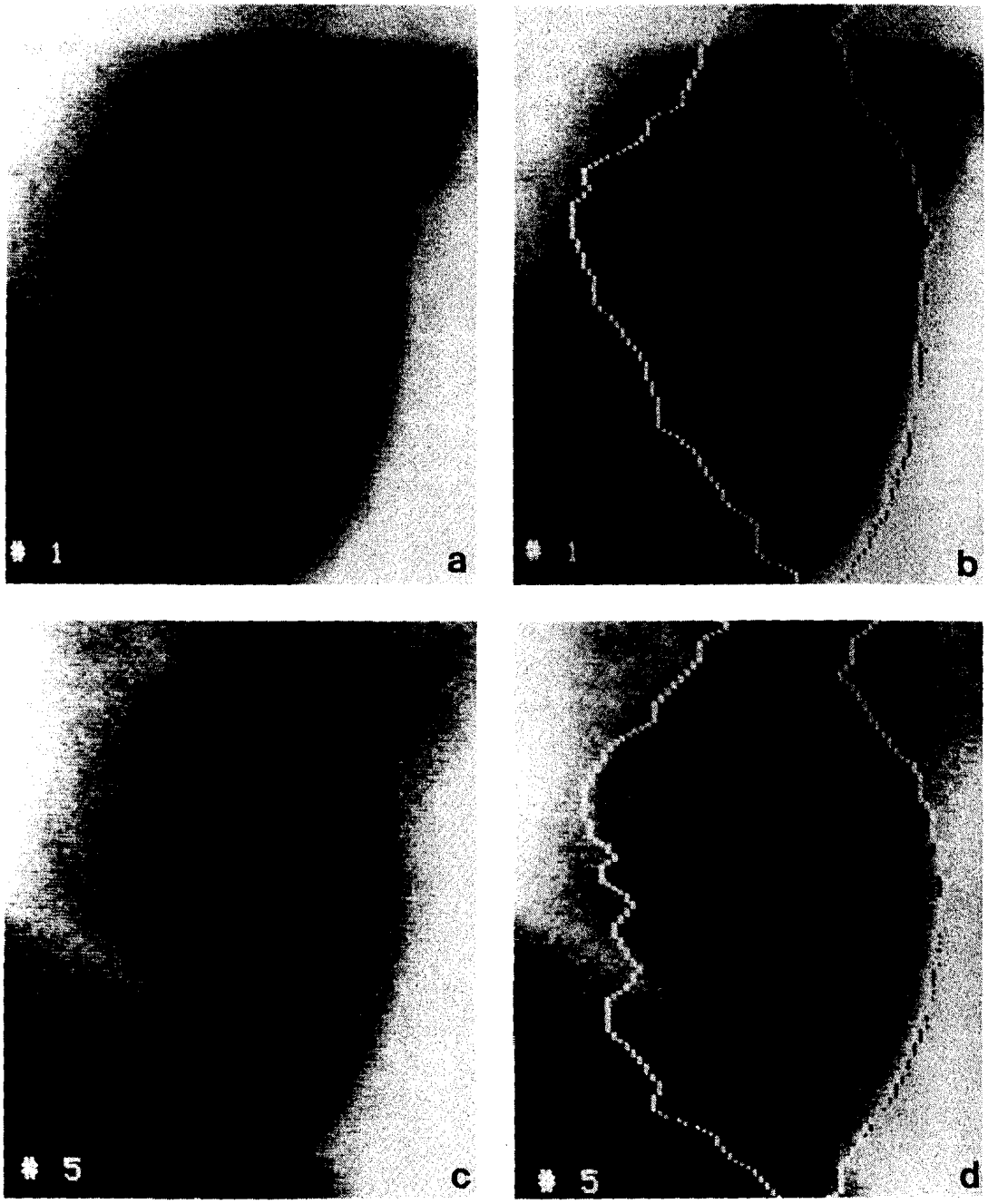

FIG. 11. (a–d) RAMTEK GX-100 displays of training images 1 and 5. The hand-traced border (black) and the computer-determined contour (white) are superimposed on the images on the right.

where manually traced contours are shown in black with computer-determined contours superimposed in white. Both images are displayed with and without contours to facilitate unbiased evaluation of results.

Computed borders agreed well with those traced by hand in 7 of the training images (including image 1, Figs. 11 a–b), while problems with segment L2 were encountered in the remaining three. This part of the ventricular wall was poorly

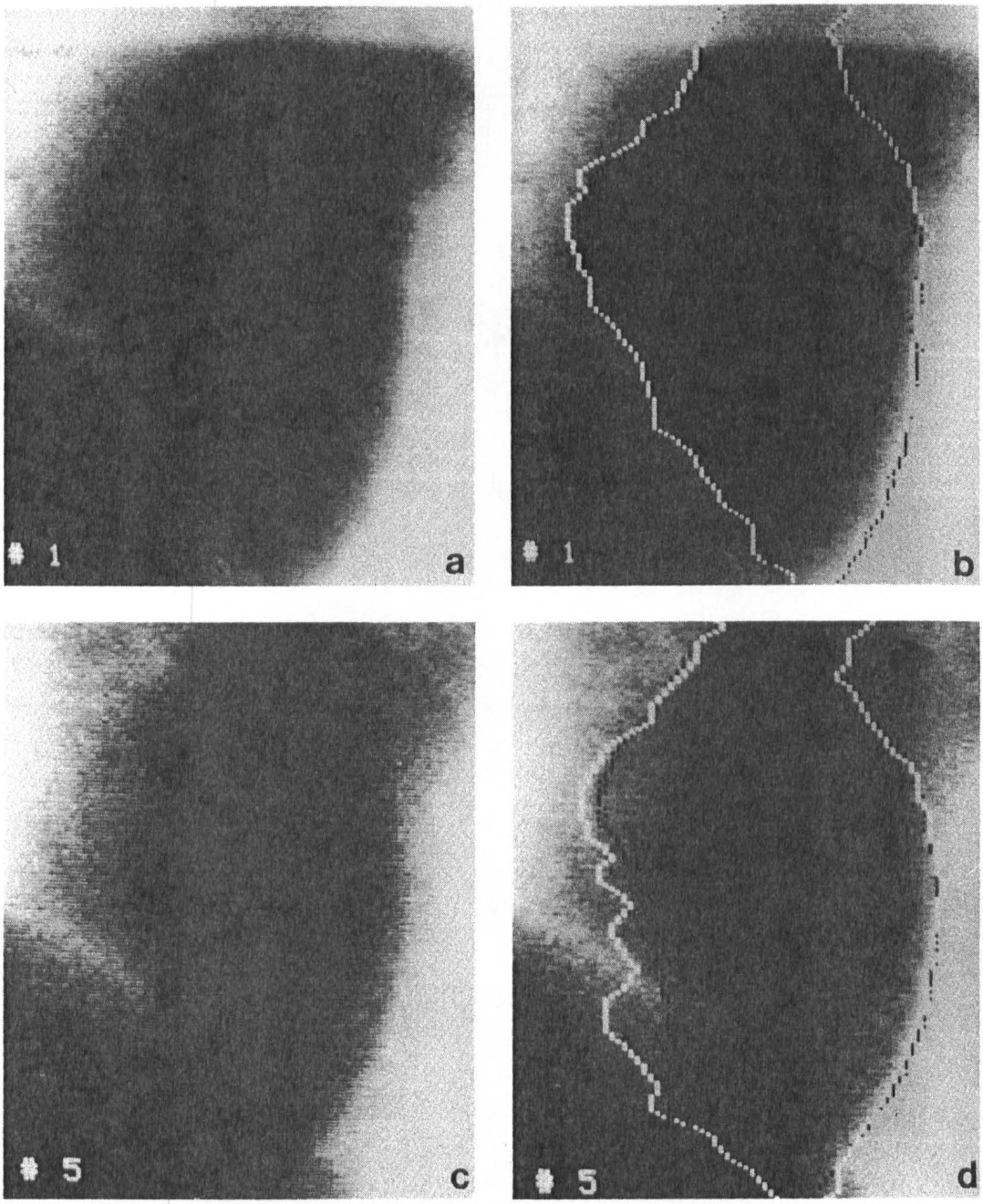

FIG. 11. (a–d) RAMTEK GX-100 displays of training images 1 and 5. The hand-traced border (black) and the computer-determined contour (white) are superimposed on the images on the right.

where manually traced contours are shown in black with computer-determined contours superimposed in white. Both images are displayed with and without contours to facilitate unbiased evaluation of results.

Computed borders agreed well with those traced by hand in 7 of the training images (including image 1, Figs. 11 a–b), while problems with segment L2 were encountered in the remaining three. This part of the ventricular wall was poorly

defined in image 5 (Figs. 11 c–d), noncharacteristic in shape in image 8, and possessed a high-contrast shadow superimposed in image 9. Minor problems were also encountered in segment L2 of image 2 where the mitral valve was significantly concave outward, in segment L1 of image 6, where the aortic valve was dramatically different in shape from that observed in the other contours, and in segment R2 of image 10, which possessed a strong gradient beyond the anterior wall.

A quantitative evaluation of the accuracy of the algorithm over all 10 cases can be obtained from the probability functions generated for the Location Predictor (Fig. 8). The frequency with which computed borders coincide with hand-traced borders, as well as the percentage of computer-determined points located within a given interval of the manually traced contour was determined from these functions and is given in Table IIA. Although only 26% of the computer-determined values were coincident with manually entered coordinates, 95% of the computed points were within a range of ±4 points or approximately 2 mm of the hand-traced borders. The mean deviation, ϵ (*13*), between computed and hand-traced borders

$$\epsilon = \Sigma \left| \frac{(\text{Hand-traced Border}) - (\text{Computed Border})}{2L} \right|, \qquad [7]$$

where L = contour length, was 1.4 points (pixels), or approximately 1.4%, since the horizontal resolution of the images is about 100 pixels. Although the mean deviation describes the overall performance of the algorithm on a given image or set of images, minor errors in the computed contour are not reflected by this

TABLE IIA

COMPARISON OF HAND-TRACED AND COMPUTER-DETERMINED BORDERS FOR TRAINING IMAGES 1–10

	Interval around hand-traced contour[a]					
Segment	0	±1	±2	±3	±4	>±4
L1	45.3	85.9	92.7	92.7	95.8	4.2
L2	22.3	57.3	77.5	89.6	94.5	5.5
L3	22.3	59.5	80.9	89.0	92.6	7.4
Left side	23.0	58.7	78.6	89.1	93.1	6.9
R1	41.0	87.5	97.6	100.0		0.0
R2	27.9	69.4	88.0	93.5	96.7	3.3
Right side	29.0	70.9	88.6	93.9	96.8	3.2
Total	26.0	64.8	83.6	91.5	95.0	5.0

[a] 1 pixel ≅0.5 mm

Note. The table shows the percentage of computed coordinates within given intervals.

measure. However, criteria for the acceptance or rejection of individual contour points can be established by measuring the reproducibility obtained from successive manual tracings of an image. Acceptable computer-determined points would be those found within this interval of reproducibility.

This interval was determined by having two observers perform five manual tracings of an end-diastolic image. Contours were averaged for each observer and mean contour points were subtracted from corresponding coordinates in each of the five manual tracings. Histograms of the differences showed that 100% of the manually entered coordinates were within ±4 points (4%) of the mean value, and that over 90% were within 1% of the mean. Since the image was well defined, similar results were obtained when contours from both observers were combined. Other studies have reported values ranging from 2 to 4% for intra- and interobserver reproducibility (*8, 13, 22*).

Since the data showed no values exceeding ±4% from the mean (the "worst-case" value reported by other observers) this interval is used as an upper limit for the acceptance or rejection of individual contour points. Using this criteria, computer-generated contours corresponding to images 1 and 4 were acceptable. Contours 2, 3, and 7 required a correction of less than 3% of the coordinates to qualify as acceptable. Those corresponding to images 5, 6, 9, and 10 required corrections of approximately 10%, and only contour 8 required a correction of more than 10% (16%) of the contour points.

In order to evaluate the effectiveness of the algorithm on a newly acquired ventriculogram, contours were computed for an additional 10 images (test set), the results of which are given in Table IIB. Using the same acceptance criteria two contours in the test set qualified, four required less than 8% correction, and

TABLE IIB

RESULTS OF BORDER ALGORITHM DERIVED FROM TRAINING IMAGES 1–10 ON TEST SET 11–20

	Interval around hand-traced contour[a]					
Segment	0	±1	±2	±3	±4	>±4
L1	31.8	55.0	67.3	68.2	74.3	26.7
L2	50.3	77.8	85.7	88.9	92.5	7.5
L3	23.6	50.2	73.0	81.7	93.7	6.3
Left side	31.8	58.5	74.7	84.3	91.5	8.5
R1	65.1	94.0	100.0			0.0
R2	31.5	70.0	83.5	89.3	94.4	5.6
Right side	35.0	72.3	85.0	90.1	95.0	5.0
Total	33.4	65.4	79.8	87.2	93.2	6.8

[a] 1 pixel ≅0.5 mm

Note. The table shows the percentage of computed coordinates within given intervals.

TABLE IIC

RESULTS OF BORDER ALGORITHM DERIVED FROM IMAGES 1–20 APPLIED TO IMAGES 1–20

	Interval around hand-traced contour[a]					
Segment	0	±1	±2	±3	±4	>±4
L1	55.7	93.1	96.2	97.2	97.8	2.2
L2	26.5	61.8	79.8	90.6	95.3	4.7
L3	21.8	54.6	75.2	84.8	89.8	10.2
Left side	25.0	58.4	77.0	86.4	91.1	8.9
R1	51.5	95.3	100.0			0.0
R2	28.6	66.3	82.4	89.7	93.6	6.4
R3	27.0	66.5	82.9	90.3	94.9	5.1
Right side	29.6	68.4	83.6	90.4	94.5	5.5
Total	27.3	63.4	80.3	88.4	92.8	7.2

[a] 1 pixel ≅0.5 mm

Note. The table shows percentage of computed coordinates within given intervals.

the remaining four required a correction of approximately 15%. These data indicate that the contour and video information obtained from the 10 training images is not completely representative. Therefore, data from the test set were included in the training set to create a more representative template and to more optimally define the probability functions associated with the four algorithmic terms. The results of the updated algorithm applied to all 20 images are given in Table IIC. Here segment R2 was split, forming an additional segment, R3. This produced a slightly better fit of the template to the anterior wall. Expansion of the training set to 20 images produced an increase in accuracy compared with the results in Table IIB, and a slight decrease in accuracy compared with those in Table IIA.

The mean time required by the algorithm to find the border in the first 10 training images was 9.8 sec, with a standard deviation of 0.79 sec.

Computer-Determined Sequential Contours

A quantitative measure of the algorithms performance on an entire contractile sequence is obtained by comparing computer-determined contours with corresponding manually traced contours, as was done for the training images. In order to avoid the tedium and time associated with 15 or 20 manual tracings, it is assumed that three fields near the beginning, middle, and end of systole will be adequate for purposes of comparison. In Fig. 12a the hand-traced and computer-determined borders for field E.D. (End-Diastole) +3 have been superimposed. A quantitative comparison indicated the computed border

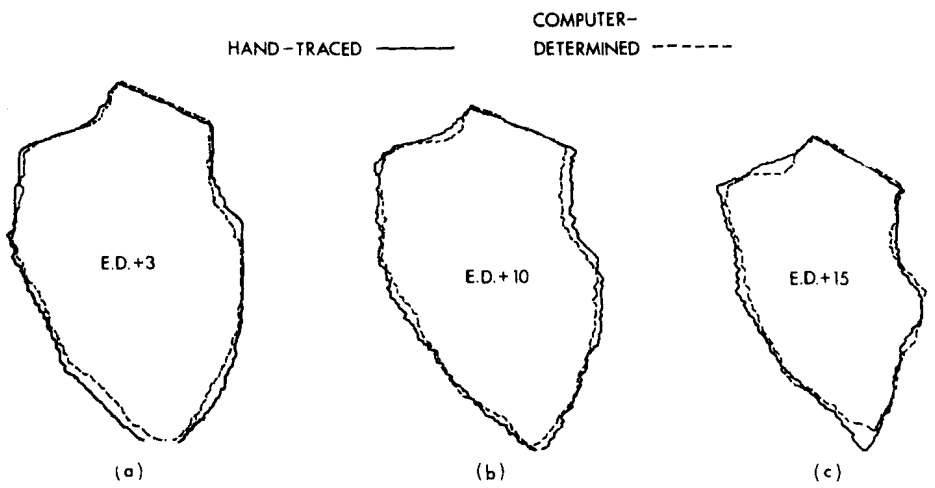

FIG. 12. Comparison of hand-traced and computer-determined contours for fields (a) E.D. + 3, (b) E.D. + 10, (c) E.D. + 15.

to be acceptable based on criteria presented previously. In Figs. 12b and c the hand-traced and computed borders have been superimposed for fields E.D. + 10 and E.D. + 15, respectively. Results showed the computer-determined contour for E.D. + 10 to be acceptable, while E.D. + 15 required a correction of approximately 3%. In order to more fully evaluate the accuracy of sequential borders, an additional nine studies such as these were performed. Each of the sequences was initialized using the algorithm developed for end-diastolic frames at which point any necessary corrections to the computer-determined contour were made. Results on beginning frames were comparable to those reported for training images 1–20. Table III indicates the percentage of computer-determined contour points which required correction in each of the 10 sequential studies performed. For the purpose of data reduction, the necessary correction is indicated only for each side rather than segmentally. As in Tables IIA–C, computed coordinates lying within ±4 points of the hand-traced contour were considered acceptable.

The authors wish to distinguish between points requiring correction and the results obtainable had the corrections actually been made. That is, the corrections which were necessary in these 10 studies were not made (with the exception of end-diastole), but instead the computer program was allowed to run until the entire systolic sequence was processed. Consequently, when an error in a given frame was made, that error was propagated in successive frames, causing the computed contour to diverge somewhat from the hand-traced border near end-systole. In practice, the computer-determined contours may be reviewed at periodic intervals, at which time any necessary corrections can be entered quickly with the use of a manually operated cursor. This prevents divergence of the contour from the ventricular wall and produces superior results as frames near end-systole are encountered.

In four of the ten sequences, 5, 6, 8, and 10, no corrections were necessary in the three frames sampled from the systolic sequence. Seven of the ten frames

TABLE III

COMPARISON OF HAND-TRACED AND COMPUTER-DETERMINED CONTOURS IN THREE DIFFERENT FIELDS SAMPLED FROM 10 SYSTOLIC SEQUENCES

	Percent correction required near								
	End-Diastole			Mid-Systole			End-Systole		
Sequence No.	Left Side	Right Side	Total	Left Side	Right Side	Total	Left Side	Right Side	Total
1	0.0	0.0	0.0	0.0	0.0	0.0	6.2	0.0	3.1
2	7.2	0.0	3.6	0.0	0.0	0.0	0.0	0.0	0.0
3	0.0	0.0	0.0	3.0	0.0	1.5	12.0	0.0	6.0
4	0.0	0.0	0.0	6.7	8.7	7.7	23.1	20.3	21.7
5	0.0	0.0	0.0	0.0	0.0	0.0	0.0	0.0	0.0
6	0.0	0.0	0.0	0.0	0.0	0.0	0.0	0.0	0.0
7	0.0	3.2	1.6	5.6	15.8	10.7	6.6	17.0	11.8
8	0.0	0.0	0.0	0.0	0.0	0.0	0.0	0.0	0.0
9	9.5	2.5	6.0	8.6	7.4	8.0	12.3	24.9	18.6
10	0.0	0.0	0.0	0.0	0.0	0.0	0.0	0.0	0.0
$\bar{x}$	1.7	0.6	1.1	2.4	3.2	2.8	6.0	6.2	6.1

encountered near end-diastole, six near mid-systole, and five near end-systole were acceptable. These data, together with mean percentage values at the bottom of Table III indicate that when necessary corrections are not made, contours will diverge slightly near end-systole.

Most of the automated techniques reported by other workers (*6–12*) do not provide a quantitative criteria for the acceptance or rejection of individual contours. However, Tasto *et al.* (*13*), in a detailed analysis of intra- and interobserver reproducibility, found a mean deviation (Eq. [7]) of 4–5 pixels when comparing computer-determined and hand-traced contours. The mean deviation found in contours 1 to 20 was approximately 1.6 pixels.

Reiber and co-workers (*14*) reported an average of 0.5 corrections per frame in the processing of sequential contours, with 45% of the corrected frames requiring only small corrections. The data in Table III indicate that 12 of the 30 frames processed needed some correction. This corresponds to 0.4 corrections per frame. A correction of 6% or less was needed in 50% of those frames requiring correction.

CONCLUSION

The results presented in Tables IIA–C and III demonstrate that the probabilistic algorithm can be successfully applied to both end-diastolic and serial left ventricular angiograms. The methods used for the development and evaluation of the algorithm include several significant features:

(1) The notion of a training set of data for control, sampling, and statistical analysis has been used extensively with computers and biomedical research. In the context of this paper, a training set consisting of pictorial information serves as a data base for developing, testing, and refining algorithmic edge-detection operations.

(2) The characterization of structural and video intensity properties using distinct probability functions and simple geometrical techniques provides a systematic approach for the translation of a priori information into algorithmic form.

(3) The probability functions derived for the parabolic template limit the search interval, thereby avoiding time and effort associated with more structured or exhaustive search techniques, while increasing the speed of the algorithm by a factor of two. The functions also predict the most probable location for the border even when no discernible information for border detection exists.

(4) Derived probability functions provide a means for evaluating the suitability of the parabolic template and probabilistic models as well as the accuracy of the resulting computer-determined borders. This not only provides a link between the two previously separate processes of data acquisition and data analysis, but also a feedback mechanism by which results can be incorporated back into the algorithm.

Technical advantages of the automated system described in this paper include:

(1) *Algorithmic flexibility*. Independence of probabilistic terms allows for extension of the algorithm through the inclusion of other border-defining criteria in the probability product.

(2) *A priori information* approximating the shape of the left ventricle is relatively invariant with respect to change in ventricular size, shape, or orientation.

(3) *Accuracy*. The algorithm found the border to be within approximately 2 mm of the hand-traced contours over 90% of the time in end-diastolic frames. In the analysis of sequential frames over 95% of the contour points were found to be within the interval of acceptance. When small corrections were required, the communications interface provided efficient interaction.

(4) *Processing Time*. The algorithm is computationally efficient, requiring less than 10 sec per contour. Processing time could be reduced considerably with the aid of a dedicated computer.

(5) *Manual Intervention* is required for digitization of the image, construction of the model, and initialization of a sequence of frames to be processed, all of which is accomplished with the same interaction.

The techniques used for the construction of the left ventricular border recognition algorithm are unique in this application but could be extended to other problems in pattern recognition as well. The concept of a probability array derived from a training set of images could be used in a number of applications where there is some observable consistency in the data.

REFERENCES

1. TSAKIRIS, A. G., DONALD, D. E., STURM, R. E., AND WOOD, E. H. Volume, ejection fraction, and internal dimensions of left ventricle determined by biplane videometry. *Fed. Proc.* **28,** 1358 (1969).
2. HEINTZEN, P. H., MOLDENAUER, K., AND LANGE, P. E. Three-dimensional computerized contraction pattern analysis. *Eur. J. Cardiol.* **1,** No. 3, 229 (1974).
3. SANDLER, H. AND DODGE, H. T. The use of single plane angiocardiograms for the calculation of left ventricular volume in man. *Amer. Heart J.* **75,** 325–334 (1968).
4. RACKLEY, C. E. Quantitative evaluation of left ventricular function by radiographic techniques. *Circulation* **54,** No. 6, 862–879 (1976).
5. CLAYTON, P. D., BULAWA, W. F., URIE, P. M., MARSHALL, H. W., AND WARNER, H. R. Quantitating left ventricular dynamics from single plane videometry. Roentgen-, Video-Techniques, "Proceedings, 2nd International Workshop Conference," p. 203. Thieme, Stuttgart, 1976.
6. ROBB, R. A. "A Computer Aided Analysis of Cardiac Dynamics Using Roentgenographic and Videometric Techniques." Ph.D. thesis, University of Utah, 1972.
7. CLAYTON, P. D., HARRIS, L. D., RUMEL, S. R., AND WARNER, H. R. Left ventricular videometry. *Comput. Biomed. Res.* **7,** 369–379 (1974).
8. COLE, J. S., HOLLAND, P. A., AND GLAESER, D. H. A semiautomated technique for the rapid evaluation of left ventricular regional wall motion. *Catheterization Cardiovasc. Diagnosis* **2,** 185 (1976).
9. COVVEY, H. D. J., ALDEMAN, A. G., FELDERHOF, C. H., TAYLOR, K. W., AND WIGLE, E. D. Television/computer dimensional analysis interface with special application to left ventricular cineangiograms. *Comput. Biol. Med.* **2,** 221 (1972).
10. CHOW, C. K. AND KANEKO, T. Automatic boundary detection of the left ventricle from cineangiograms. *Comput. Biomed. Res.* **5,** 388 (1972).
11. SMALLING, R. W., SKOLNICK, M. H., MYERS, D., SHABETAI, R., AND COLE, J. C. Digital boundary detection, volumetric and wall motion analysis of left ventricular cine angiograms. *Comput. Biol. Med.* **6,** 73 (1976).
12. MODESTINO, J. W., ASHKAR, G. P., FRIES, R. W., AND KAUFMAN, H. Computer evaluation of dynamic left ventricular volume from serial angiocardograms. *In* "Computers in Cardiology," p. 211. IEEE, 1976.
13. TASTO, M., FELGENDREHER, M., SPIESBERGER, W., SPILLER, P., AND HAMBURG, F. R. G.: Comparison of manual versus computer determination of left ventricular boundaries from X-ray cineangiocardiograms. Roentgen-, Video-Techniques. "Proceedings, 2nd International Workshop Conference," p. 168, Thieme, Stuttgart, 1976.
14. REIBER, J. H. C., SLAGER, C. J., SCHUURBIERS, J. C. H., AND MEESTER, G. T. Contouromat—A hard wired left ventricular angio processing system. II. Performance evaluation. *Comput. Biomed. Res.* **11,** 503, 523 (1978).
15. PERSOON, E. A new edge detection algorithm and its applications in picture processing. *Computer Graphics and Image Processing* **5,** 425–446 (1976).
16. GRIFFITH, A. K. Edge detection in simple scenes using a priori information. *IEEE Trans. Computers* **C-22,** 371–381 (1973).
17. CHIEN, Y. P. AND FU, K. S. A decision function method for boundary detection. *Computer Graphics and Image Processing* **3,** 125–40 (1974).
18. RUMEL. S. R. "A Computer Interactive Videodigitizer." Masters thesis, University of Utah, 1973.
19. BARRETT, W. A., CLAYTON, P. D., AND WARNER, H. R. A system for evaluation and refinement of left ventricular border recognition algorithms. *In* "Computers in Cardiology," p. 251. IEEE, 1976.
20. BARRETT, W. A. "A Stochastic Model for Probabilistic Determination of Left Ventricular Borders." Ph.D. thesis, University of Utah, 1978.

21. PARZEN, E. "Modern Probability Theory and its Applications," 1st ed., pp. 151–176. Wiley, New York, 1960.
22. CHAITMAN, B. R., DEMOTS, H., BRISTOW, J. D., ROSCH, J., AND RAHIMTOOLA, S. H. Objective and subjective analysis of left ventricular angiograms. *Circulation* **52,** 420–425 (1975).